

# TESSELLATE asteroids paper

Brayden Leicester, Ryan Ridden-Harper, Michele Bannister and Others

September 16, 2025

## 1 Abstract

## 2 Introduction

Since 2017, the Transiting Exoplanet Survey Satellite (*TESS*, Ricker et al., 2014) has been observing large swathes ( $96^\circ \times 24^\circ$ ) of sky at a very high cadence. These month long blocks of full frame images (FFIs) are named sectors, with the cadence of the sectors dependant on the cycle. The cadence started at 30 min, then increased to 10 min, and has now increased again to 200 s FFIs.

The large archival dataset of *TESS* has gone largely unanalysed. This is until the **TESSELLATE** project (H. Roxburgh and R. Ridden-Harper et al. 2025), which seeks to find all the transient events that were serendipitously observed by *TESS*. **TESSELLATE** searches every pixel of every FFI from *TESS*, using the **TESSreduce** (Ridden-Harper et al., 2021b) to looking for changes in brightness that could be related to a physical event.

Asteroids are the most numerous source of non-transient detections in **TESSELLATE**, and need to be filtered out of the rest of the data. This also allows for analysis of the properties of these planetesimals. This letter presents our analysis of the asteroids found with the first set of **TESSELLATE** sectors, with a 10 min cadence. This cadence is fast enough that the Nyquist frequency of the observations is above the spin barrier for asteroids (Pravec & Harris, 2000), so *TESS* could detect new fast rotators.

There have been other studies done using *TESS* to characterise asteroids. It was suggested by Pál et al. (2018) that it would be possible to get good photometry down to  $V \lesssim 19$  mag. They followed up with an analysis of the small bodies the first 12 sectors (cycle 1) (Pál et al., 2020), tripling the number of asteroids with accurate rotation periods. McNeill et al. (2023) re-analyses the same sectors of cycle 1, and is in broad agreement with Pál et al..

*TESS* is used for solar-system observation in many other ways aswell. The Minor Planet Center (MPC) gets regular updates on asteroids in *TESS* from the **LINEAR-TESS** program (Woods et al., 2021). Gowanlock et al. (2024) uses *TESS* photometry as well as observations by the Zwicky Transient Facility (ZTF, Bellm et al., 2019) to get a longer baseline on mutually observed objects while combining ground and space-based observations. Single object analysis is also possible, Humes & Hanuš (2024) recover the period of an asteroid commensurate with Earth’s rotation. They also use the *TESS* data alongside other observations to determine the shape of the object. *TESS* has been used to study comets as well (e.g. Ridden-Harper et al., 2021a) Fainter and unknown solar system objects can be found by shift and stacking (Holman et al., 2019, Payne et al., 2019, Rice & Laughlin, 2020) or taking a fast X-ray transform (Nguyen et al., 2024) of the *TESS* FFI data.

For our analysis of the asteroids in *TESS*, we use the third year of observations from the spacecraft; sectors 27 to 39. These were the first sectors to have a 10 min cadence. Our methods are presented in section 3, followed by the results in section 4. A discussion of how our results compare to other *TESS* asteroid studies is given in section 5, and we conclude in section 6.

### 3 Methods

**TESSELLATE** provides a new way to find and characterize asteroids: detecting them as transient events. The lightcurves of these detections often have spike only a few frames long, as the asteroid moves over the pixel of interest. Asteroids move at about 1 px per frame for the 30 min cadence (Pál et al., 2018), and thus are found as many different transient events as they cross a sector. Both **SourceDetect** and **Starfind**, the detection methods employed by **TESSELLATE**, detect planetesimals.

Characterizing the spikes in the single pixel lightcurves as an “asteroid” has its problems, as real transient events can look similar. We have implemented another way of finding and removing asteroids from the set of detected events. The reduction of full sectors during a **TESSELLATE** run also allows for forced photometry at known asteroid positions. These can then be matched with the detections to classify the spikes, and properties of the asteroids can be measured at the same time.

The position of known asteroids is important for matching them to detections. We use **SkyBoT** (Berthier et al., 2006) coneseach to find all the asteroids with  $V \leq 20$  mag, the limit suggested by (Pál et al., 2018). We query every 12 h over the month of the sector, and interpolate the positions to the times of the *TESS* observations. With *TESS*’s large pixel scale, these interpolations are accurate enough for our purposes, and save on time and resources, as the query can be expensive.

The positions of these asteroids can be matched with the detections, using a **KDTree** (Manee-wongvatana & Mount, 1999). Setting boundaries of 0.1 d and 1 px on the nearest match keeps only objects that are coincident temporally and spatially. If two such objects match to the same detection, the shortest distance between the positions is taken. The matched events are then classified as asteroids, and are not considered further by **TESSELLATE**.

Forced photometry along the tracks of the asteroids allows for the construction of lightcurves. The differenced images are used for the forced photometry, as the objects are moving they are not dimmed by the differencing. Aperture photometry, using **Photutils** (Bradley et al., 2024), is performed at the centre of mass of the point spread function with a 1.5 px aperture, the standard size of an aperture in **TESSELLATE**. The lightcurves are then sigma-clipped to  $3\sigma$  from the mean remove background stellar contamination.

From their lightcurves, the rotation period of the object can be determined by using a Lomb-Scargle periodogram (Lomb et al. (1976), Scargle et al. (1982), but see VanderPlas, 2018, for a review). The new **NIFTY-LS** package (Garrison et al., 2024), as implemented in **astropy** (Astropy Collaboration et al., 2013, 2018, 2022), was used to calculate the periodogram. The periodogram searched for rotation periods between the Nyquist limit of 20 min and a maximum of 17 d (the value used in McNeill et al., 2023, due to the length of the lightcurve). The uncertainty in the frequency is calculated as half full width half maximum of the peak found in the periodogram, crudely approximating the peaks as Gaussian.

-Example Figure

An example of the periodogram fit to the lightcurve is given by Figure 1. A clear maximum power is found in the top panel, and the associated frequency is fed to the model shown in the

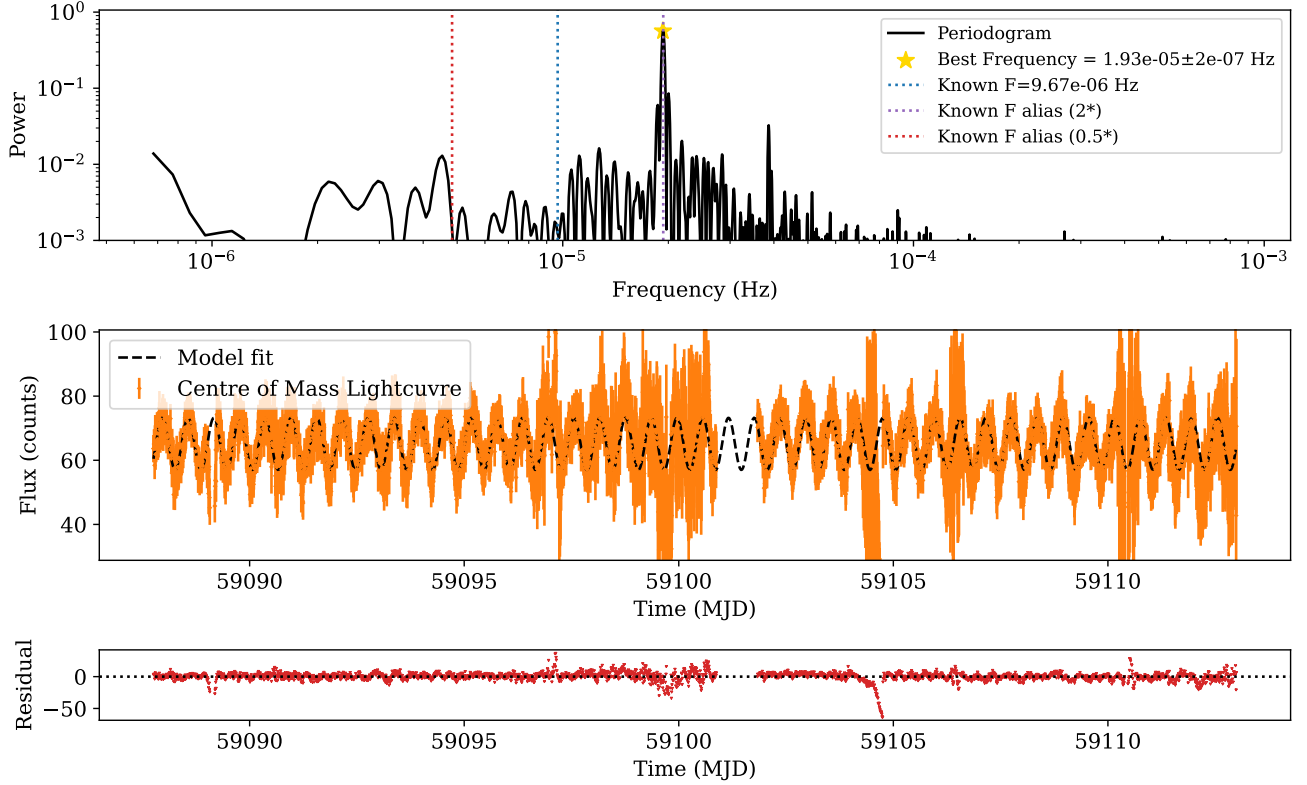


Figure 1: An example of the periodogram analysis we conduct for each object. This figure uses the lightcurve of the asteroid (5254) Ulysses from sector 29. Top panel: A periodogram of the lightcurve, with the known frequency and aliases indicated (from the LCDB). Middle panel: The lightcurve (orange error bars) and model(dashed black). Lower panel: Residuals of the difference between the model and the lightcurve.

middle panel. The residuals in the lower panel are small for the most part, with large deviations from zero only where the lightcurve has large uncertainty in its flux. Thanks to the known frequency from LCDB plotted, we note that we recover the double frequency alias, this is explored further below.

#### -Quality Checks on the lightcurves

Not every lightcurve is good enough for analysis, so some quality cuts are applied to the lightcurves. A minimum brightness cut of 10 counts ( $m_T \sim 18$  mag) is applied, otherwise the lightcurve is indistinguishable from noise. Following McNeill et al., we do not trust the periods of any lightcurve with  $\leq 200$  data points.

There were also quality cuts applied to the periodograms. The methods would return the 17d maximum value if no physical period was detected, so also following McNeill et al. (2023) we discard any periods within 10% of this maximum. They find that periods of  $\leq 3$  h is also unreliable. We are using data with a factor of three higher cadence, so we reduce this condition to  $\leq 1$  h for the same number of observations sampled per rotation.

The above methods are integrated into the rest of the TESSELLATE pipeline. This allows for asteroids to be filtered out of the new detections as they happen. The results given below will be improved upon as more sectors are run and a higher number of minor planets can have their rotation properties measured.

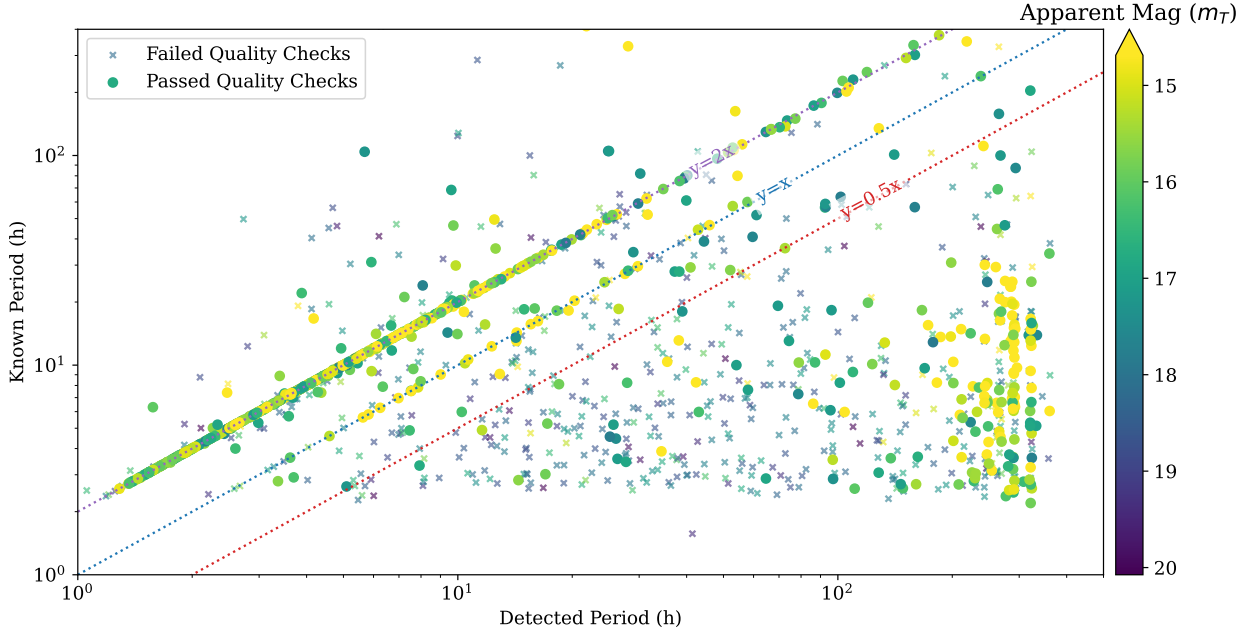


Figure 2: Comparison of the detected period and known period for all the asteroids analysed that are in the LCDB. Those that failed the quality check are shown with crosses, and those that passed are filled circles. They are coloured by the measured mean *TESS* magnitude ( $m_T$ ). The 1:1 correspondence line (blue), and the factor of two aliases (purple ( $\times 2$ ) and red ( $\times 0.5$ )) are plotted as dotted lines.

## 4 Results

-Total Asteroids found

57426 of asteroids with  $V \leq 20$  mag were found in the year 3 sectors we analysed. Most of these are too faint for the lightcurve to give a reliable and period, while Pál et al. (2018) thinks good photometry down to  $V \lesssim 19$  mag should be achievable, we find the limit for TESSELLATE is closer to  $m_T \approx 17$  mag (H. Roxburgh and R. Ridden-Harper et al. 2025). Once the quality checks (described above) have been applied, we are left with 4328 of planetesimals with accurate rotation rates. 80% of these asteroids do not have reliable periods reported in the LCDB, so we are the first to get the rotation period for these bodies.

-Properties of those that pass

57426 total, 1530 in LCDB, 868 of those pass check, 581 within 5 percent of  $y=2x$ , 28 within 5 percent of  $y=x$

We present double the periods we detect from periodograms as the rotation rate of these objects. This is because  $\approx 70\%$  of the asteroid that pass the quality checks in Figure 2 line within 5% of the  $y = 2x$  line; they have double peaked lightcurves. A few percent have the same period detected as in the LCDB, but a larger fraction have periods detected with no relation to their known period. Extrapolating this trend to the 4328 asteroids that pass the checks, we present an accurate rotation period for  $\sim 3030$  of them (unfortunately we cannot say which ones).

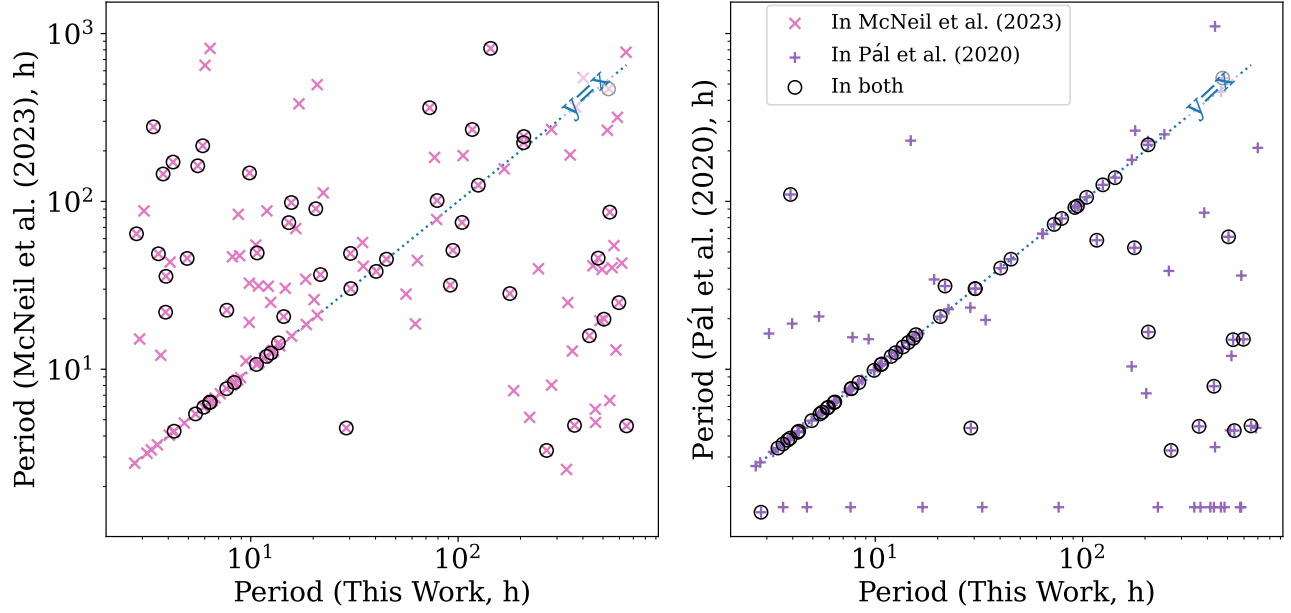


Figure 3: Comparing the rotation period of asteroids found in this work to asteroids in other studies that used TESS to investigate asteroids. Left: The comparison to McNeill et al. (2023) plotted as pink crosses, there are **139** objects. Right: The comparison to Pál et al. (2020) plotted as purple pluses, there are **117** objects. Those planetesimals found in all three works are circled (**54** asteroids). Lines of 1:1 agreement are plotted (dotted blue).

## 5 Discussion

-Comp to Pal and McNeill

Figure 3

-Fast Rotator Plot

We do not find any fast rotators in our dataset. This is encapsulated by none of our objects being above the spin barrier shown in Figure 4.

While our Nyquist limit is well above the spin barrier of Pravec & Harris (2000) thanks to *TESS*’s fast cadence, most asteroids discovered above the barrier are small, and therefore dim. The shallow magnitude of *TESSELLATE* (Roxburgh et al., 2025) makes it difficult for dim planetesimals to pass the quality checks.

-other discussion

The rotation periods of the brightest asteroids are not recovered. This is due to the fixed aperture size of our forced photometry, 1.5px. The bright asteroids can start to saturate the *TESS* detector, and can bloom out to occupy more pixels. We chose to keep a constant aperture to standardise the analysis, and to be agnostic to the properties of the asteroid being analysed.

Some asteroids slip through our detection methods, and end up unclassified in the *TESSELLATE* data. This is often because the detections of bright asteroids are offset from the predicted positions by further than the matching radius we set. Asteroids are easy to spot for our Cosmic Cataclysms Zooniverse<sup>1</sup> volunteers, as they are at a different position in the “1 hour later” panel, so any that slip past can be caught here.

<sup>1</sup> <https://www.zooniverse.org/projects/cheerfuluser/cosmic-cataclysms>

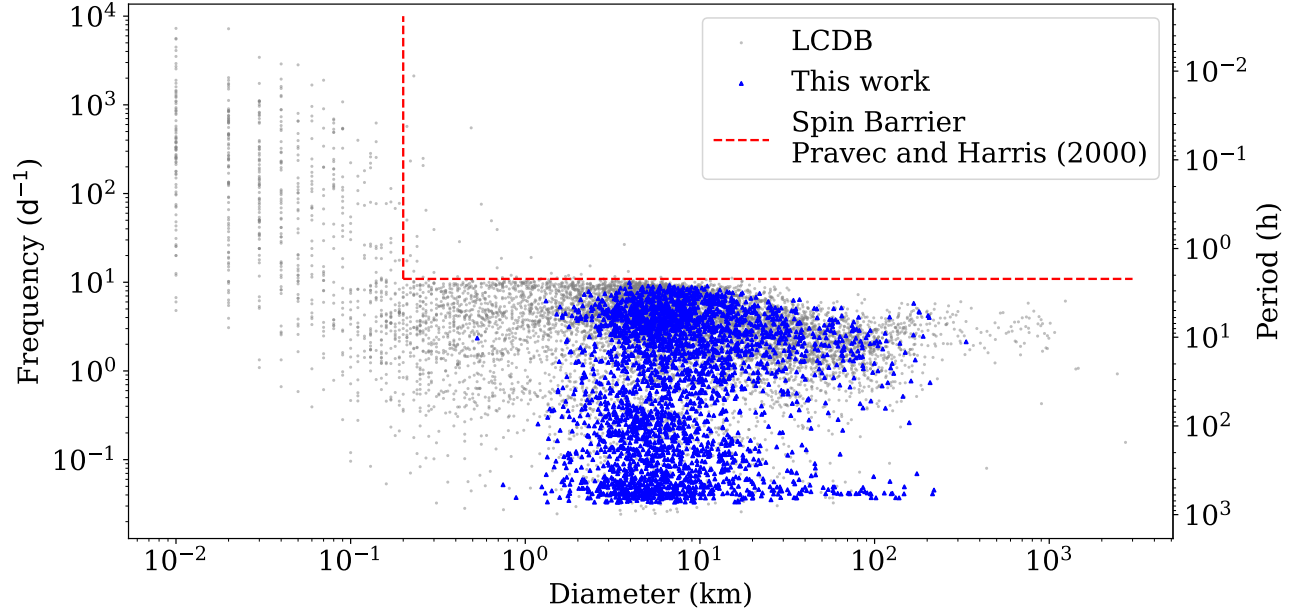


Figure 4: A rotation rate against size plot after the LCDB (Warner et al., 2009) (grey circles) with this work’s addition (blue squares). The diameters are from NEOWISE (Masiero et al., 2011, Mainzer et al., 2019) where available. The red dashed lines represent the spin barrier of (Pravec & Harris, 2000).

## 6 Conclusion

## References

- Astropy Collaboration, Robitaille, T. P., Tollerud, E. J., et al. 2013, *Astronomy and Astrophysics*, 558, A33, doi: 10.1051/0004-6361/201322068
- Astropy Collaboration, Price-Whelan, A. M., Sipőcz, B. M., et al. 2018, *AJ*, 156, 123, doi: 10.3847/1538-3881/AABC4F
- Astropy Collaboration, Price-Whelan, A. M., Lim, P. L., et al. 2022, *ApJ*, 935, 167, doi: 10.3847/1538-4357/AC7C74
- Bellm, E. C., Kulkarni, S. R., Graham, M. J., et al. 2019, *Publications of the Astronomical Society of the Pacific*, 131, 018002, doi: 10.1088/1538-3873/aaecbe
- Berthier, J., Vachier, F., Thuillot, W., et al. 2006, *ASPC*, 351, 367. <https://ui.adsabs.harvard.edu/abs/2006ASPC..351..367B/abstract>
- Bradley, L., Sipőcz, B., Robitaille, T., et al. 2024, *astropy/photutils*: 1.13.0, Zenodo, doi: 10.5281/zenodo.12585239
- Garrison, L. H., Foreman-Mackey, D., hsuan Shih, Y., & Barnett, A. 2024, *Research Notes of the AAS*, 8, 250, doi: 10.3847/2515-5172/ad82cd

- Gowanlock, M., Trilling, D. E., McNeill, A., Kramer, D., & Chernyavskaya, M. 2024. <http://arxiv.org/abs/2408.04096>
- Holman, M. J., Payne, M. J., & Pál, A. 2019, Research Notes of the AAS, 3, 160, doi: 10.3847/2515-5172/ab4ea6
- Humes, O. A., & Hanuš, J. 2024, arXiv, arXiv:2412.04123, doi: 10.48550/ARXIV.2412.04123
- Lomb, N. R., Lomb, & R., N. 1976, Ap&SS, 39, 447, doi: 10.1007/BF00648343
- Mainzer, A., Bauer, J., Cutri, R., et al. 2019, NEOWISE Diameters and Albedos V2.0, NASA Planetary Data System, doi: 10.26033/18S3-2Z54
- Maneewongvatana, S., & Mount, D. M. 1999, arXiv, cs/9901013, doi: 10.48550/ARXIV.CS/9901013
- Masiero, J. R., Mainzer, A. K., Grav, T., et al. 2011, Astrophysical Journal, 741, 68, doi: 10.1088/0004-637X/741/2/68
- McNeill, A., Gowanlock, M., Mommert, M., et al. 2023, The Astronomical Journal, 166, 152, doi: 10.3847/1538-3881/ACF194
- Nguyen, T., Woods, D. F., Ruprecht, J., et al. 2024, AJ, 167, 113, doi: 10.3847/1538-3881/AD20E0
- Payne, M. J., Holman, M. J., & Pál, A. 2019, Research Notes of the AAS, 3, 172, doi: 10.3847/2515-5172/ab5641
- Pravec, P., & Harris, A. W. 2000, Icar, 148, 12, doi: 10.1006/ICAR.2000.6482
- Pál, A., Molnár, L., & Kiss, C. 2018, Publications of the Astronomical Society of the Pacific, 130, 114503, doi: 10.1088/1538-3873/aae2aa
- Pál, A., Szakáts, R., Kiss, C., et al. 2020, The Astrophysical Journal Supplement Series, 247, 26, doi: 10.3847/1538-4365/ab64f0
- Rice, M., & Laughlin, G. 2020, Planetary Science Journal, 1, 81, doi: 10.3847/PSJ/abc42c
- Ricker, G. R., Winn, J. N., Vanderspek, R., et al. 2014, Journal of Astronomical Telescopes, Instruments, and Systems, 1, 014003, doi: 10.1117/1.JATIS.1.1.014003
- Ridden-Harper, R., Bannister, M. T., & Kokotanekova, R. 2021a, Research Notes of the American Astronomical Society, 5, 161, doi: 10.3847/2515-5172/ac1512
- Ridden-Harper, R., Rest, A., Hounsell, R., et al. 2021b, arXiv e-prints, arXiv:2111.15006. <https://arxiv.org/abs/2111.15006>
- Roxburgh, H., Ridden-Harper, R., Moore, A., et al. 2025, arXiv e-prints, arXiv:2502.16905, doi: 10.48550/arXiv.2502.16905
- Scargle, J. D., Scargle, & D., J. 1982, ApJ, 263, 835, doi: 10.1086/160554
- VanderPlas, J. T. 2018, The Astrophysical Journal Supplement Series, 236, 16, doi: 10.3847/1538-4365/aab766

- Warner, B. D., Harris, A. W., & Pravec, P. 2009, *Icar*, 202, 134, doi: 10.1016/J.ICARUS.2009.02.003
- Woods, D. F., Ruprecht, J. D., Kotson, M. C., et al. 2021, *PASP*, 133, 014503, doi: 10.1088/1538-3873/ABC761